Nickel and Iron Biocarbon Catalysts for Water-Gas Shift Reaction

Graul Théodore, González Martínez María, Nzihou Ange

Nickel and Iron Biocarbon Catalysts for Water-Gas Shift Reaction

Graul Théodore[1] · **González Martínez María**[1] · **Nzihou Ange**[1]

Abstract

Biocarbon catalysts for water-gas shift (WGS) reaction were prepared from pyrolyzed fern (F) impregnated with iron (Fe) and nickel (Ni) salts. They were tested in a fixed-bed reactor from 180 °C to 400 °C with variable steam to carbon mon-oxide (S/CO) ratio (1.4 to 20.7) and compared to rust. CO conversion was mostly below 10% and favored by increasing temperature and steam partial pressure relative to WGS kinetics. Ni-biocarbon catalysts were more active for WGS due to their lower temperature activity, according to their reducibility and inherent metals which improved electronic proper-ties. WGS selectivity was generally above 95%, reflecting WGS predominance over methanation. FNiFe-B (impregnated before pyrolysis) was the most performant catalyst (10.3% conversion, 99.7% selectivity, 280 °C). Maximal rust conver-sion was 6.9% at 280 °C, compared to 20% at 300 °C in the literature. Catalyst activation energy and pre-exponential fac-
tor of 92.1 kJ/mol and 2.2×10^8 respectively were determined, and comparable to literature (up to 130 kJ/mol; 5.8×10^{10}). Low temperature activity provided by Ni combined with Fe and fern-inherent metals' co-catalytic effect was reflected in the high WGS performance by FNiFe-B with its associated kinetic parameters (59.5 kJ/mol; 5.6×10^5).

Highlights

- Biocarbon catalysts were more active than rust for water gas shift reaction (WGS).
- Ni-biocarbon catalysts were more active than Fe-biocarbon catalysts for WGS.
- WGS was kinetically driven and enhanced with increased temperature and steam.
- Biocarbon catalyst reduction could enhance catalyst performance in WGS.

[1] Université de Toulouse, Mines Albi, CNRS UMR 5302, Centre RAPSODEE, Campus Jarlard, Route de Teillet, Albi 81000, France

Graphical Abstract

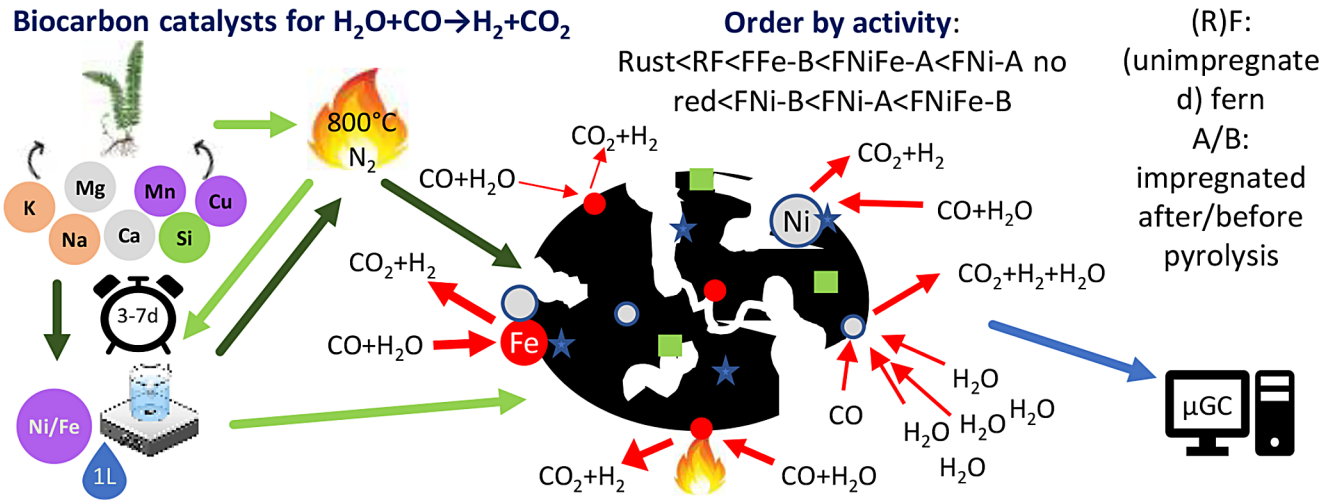

Keywords Biocarbon · Catalyst · Water-gas shift · Iron · Nickel

Statement of novelty

Most of the current catalysts have high environmental impacts caused by solvent and energy-intensive processes. This work presents an eco-friendly alternative, through the use of biocarbon catalysts. Fern was pyrolyzed and impregnated with iron and nickel and tested in water-gas shift reaction. In the reaction conditions, the fern-based catalysts outperformed rust (Fe_2O_3), revealing the potential of biocarbon catalysts.

Abbreviations

BC	Biocarbon or biochar
BET	Brunauer–Emmett–Teller
BM	Biomass
cat.	Catalyst
CHNS	Carbon, hydrogen, nitrogen, sulfur
GHG	Green-house gas
GHSV	Gas hourly space velocity
ICP-AES	Inductively coupled plasma atomic emission spectroscopy
IWI	Incipient wetness impregnation
P	Pressure
pr.	Promoter
PR-BM	Peng Robinson – Boston Mathias
r	Kinetic rate
RSD	Relative standard deviation
RWGS	Reverse water-gas shift reaction
S	Selectivity
S/C or CO	Steam to carbon or carbon monoxide ratio
SEM	Scanning electron microscopy
sup.	Support
T	Temperature
TEM	Transmission electron microscopy
TGA-DSC	Thermogravimetric analysis – differential scanning calorimetry
TPD	Temperature programmed desorption
TPO	Temperature programmed oxidation
TPR	Temperature programmed reduction
$\dot{V}$	Volumetric flow
WGS	Water-gas shift
WI	Wetness impregnation
X	Conversion
XRD	X-ray diffraction

Introduction

Human-caused climate change is accelerating and results in scarcer food and water availability, deteriorated health and well-being, harsher and more frequent damage to infrastructure and ecosystems. This shift is a result of green-house gas (GHG) emissions mainly carbon dioxide (CO_2) and their mitigation can help minimize present and future impacts.

The production of low-emission hydrogen (H_2) and H_2 derivatives through biomass and biowaste valorization could mitigate the use of fossil fuels in GHG intensive sectors [1]. H_2 can be synthesized in gas produced from thermochemical conversion (500 to 1000 °C, inert atmosphere). Water-gas shift (WGS, Eq. 1) reaction is involved in thermochemical conversion pathways and allows improved hydrogen content in syngas thanks to steam ($(H_2O)_v$) (180–500 °C).

$$\begin{aligned} &CO + (H_2O)_v \leftrightarrow CO_2 + H_2 \\ &\Delta H^0_{298} = -41.2\, kJ/mol \end{aligned} \quad (1)$$

Thermochemical conversion reactions can be catalyzed using noble or transition metal-based catalysts including iron (Fe) and nickel (Ni). They reduce reaction temperature, process production cost and lowers H_2 production costs while favoring its accessibility [2–4]. These reactions include low temperature WGS, which is an exothermic reaction kinetically restricted due to energy barriers that can be lowered through catalysis [5–7]. These processes are complex and imply many competitive reactions resulting in unwanted byproducts. This is the case of CH_4 formation through methanation (Eq. 2), which is a more exothermic reaction compared to WGS and thus rivals CO_2 then H_2 formation by WGS [8, 9].

$$\begin{aligned} &CO + 3H_2 \leftrightarrow \ \ CH_4 + H_2O \\ &\Delta H^0_{298} = -206.0\, kJ/mol \end{aligned} \quad (2)$$

The metal extraction for metallic catalyst production has a high environmental impact due to energy and solvent intensive processes that emit GHG. This effect is worsened for noble metals, that are costlier due to scarcity, but more active as catalysts [10–13]. To minimize the extraction's influence, catalysts are being derived from inherently rich or loaded in metal bioresources [14].

The reaction kinetics can be expressed through the determination of the reaction rate (r) based on theoretical calculations (Langmuir-Hinshelwood, power law, etc.) validated through experimental data. The one used in this article is the power law expression (Eq. 3) [15–17].

$$r = kP^a_{CO}P^b_{H_2O}P^c_{CO_2}P^d_{H_2} \quad (3)$$

The kinetic constant (k) is obtained by Arrhenius type equations (Eq. 4). They are defined by their pre-exponential factor (A or k_0, unit depending on reaction order) and the activation energy (E or E_a, kJ or kcal/mol) [18, 19]. Based on this equation, the rate and thereafter conversion of CO are increased by diminishing E_a or increasing k_0. Both kinetic parameters are also impacted by temperature.

$$k = \ k_0 \times \ e^{-\frac{E_a}{RT}} \quad (4)$$

Non-noble catalysts such as Ni catalysts supported by MgAl, Mg, Al and CaAl could promote WGS with E_a ranging 67 to 186 kJ/mol and k_0 spanning 5.4×10^4 to 4.3×10^{12}. Side reactions methanation and steam methane reforming can be catalyzed simultaneously with E_a ranging from 33 to 244 kJ/mol and k_0 from 5.5×10^3 to 1.2×10^{16} for both reactions [20]. Over $CuO/ZnO/Al_2O_3$ and depending on the equation used to calculate initial rates, E_a can range from 28.5 to 92.9 kJ/mol and k_0 from 2.6×10^4 to 5.8×10^{10} [15].

Abundant literature is available on the kinetic parameters regarding Cu, Fe, Ru, Ni, Rh, Pd and Pt-based catalysts. This results in activation energies between 0.5 and 130 kJ/mol and pre-exponential factors between 5.4×10^{-7} to 1.5×10^{10} [17, 21, 22]. The variability in values obtained for these kinetic parameters stems from aforementioned promotion and support effects that decrease E_a. This metallic addition can also prevent the sintering of metal phases which could result in CO and H_2O reactivity loss. Also, different catalysts react differently with the gases. They then undergo specific reaction mechanisms (associative, redox, Langmuir-Hinshelwood) that take into account their active sites and result in specific methods to determine kinetic parameters [16, 23, 24]. Highly dispersed nanosized active sites could be beneficial for WGS and result in faster kinetics at lower temperatures as the smaller sized active site does not require as much energy to be activated [16, 25, 26]. These mechanisms could involve a redox couple of a same metal that undergoes a switch from the oxidant to the reductant and inversely, which can be facilitated through activation [16, 27]. Including possible reducible active phases, the speciation can determine WGS reactivity as a covalent bond could be less polarized with more reactive electrons compared to ionic bonds. Additionally, the engaged orbitals could limit the direction of reaction with gases, especially for clusters that have less electron back-donation. As they cannot densely engage electrons, this weakens its gas activation and consequently kinetic capabilities [16, 24, 25]. Other sources of uncertainty were attributed to gas impurities, mass-diffusion limitations and the type of reactor related to pressure gradients that locally affect kinetics and inhibit or poison WGS and active sites [16, 23, 27].

The operating conditions can also affect the WGS reaction. Increasing temperature provides the energy to activate chemicals and molecules, improves WGS kinetics but inhibits thermodynamic equilibrium (exothermicity) and facilitates the change of electronic state of metals that could also sinter [28, 29]. The excess of steam to carbon monoxide (CO) or carbon (S/C) also displaces the equilibrium of the reaction towards the formation of products H_2 and CO_2 by reactant excess, but could deactivate catalysts faster [30, 31]. Lastly, a low gas hourly space velocity (GHSV) provides sufficient time to allow the gases to react with the active sites of the catalyst [32].

The objective of this work is therefore to produce, characterize and test biocarbon catalysts from bioresources loaded with heavy metals whose catalytic activity was identified for WGS with low activation energy and high pre-exponential factor. The efficiency of this approach has been proven in reverse WGS [33]. In this work, the impact of the catalyst,

temperature, S/C, and indirectly GHSV were chosen. Other factors not modified here such as pressure, contact time, choice of reactor, its configuration and its accessories (such as permeation and chemisorption devices) can also have an important effect on the process [19, 34, 35].

Materials and Methods

Preparation and Utilization of the Biocarbon Catalysts

In a first approach, fern and willow were selected as raw bioresources known for their ability to accumulate heavy metals from soil by phytoremediation. Willow was harvested in the South of France in 2015. Fern corresponds to shrublands mainly composed of fern harvested in Brittany (France) in 2019.

To mimic heavy metal content in phytoremediation, both biomass and biocarbon were impregnated with Ni and Fe nitrate ($Ni(NO_3)_2{\cdot};6H_2O$ and $Fe(NO_3)_3{\cdot};9H_2O$) to reach a metal load of 30 mg per g of biocarbon. As a result, we obtained biocarbon catalysts impregnated before and after pyrolysis. Biocarbon was produced by raw (RF and RW for fern and willow) or impregnated biomass pyrolysis under 1 L/min nitrogen (N_2) from 25 °C to 800 °C, at 2 °C/min, followed by an isothermal step at 800 °C for an hour. Wetness impregnation (WI) was applied to raw biomass: 20 g of biomass was submerged in different 1 L aqueous solutions containing Fe or Ni nitrates, stirred for 3 days and then dried for 1 day at 60 °C [11]. WI based on incipient WI (IWI) was applied to biocarbon: wettable volume and amount of nitrate to attain a fixed percentage of metal in biocarbon helped determine a concentration of nitrate to thereafter be replicated in 100mL of water for 2 g of biocarbon [36]. The solutions were stirred for varying amounts and time and then dried for 1 day at 60–105 °C. The final nickel and iron composition of the biocarbon catalysts was measured by ICP-OES (Table 1).

Biocarbon catalysts were then tested for WGS reaction in a fixed bed reactor (Top Industries (France), 8 mm diameter, 25 cm long, Fig. 1). The reactor was filled with the catalyst and an inert bed of alumina (θ-Al_2O_3, [37]), which allowed fixed catalyst position in the isothermal area of the reactor [36, 38]. Moisture was removed before reaction by flowing argon (Ar) at 120 °C during 1 h. Samples were then pre-reduced under 60vol%/40vol% H_2/Ar at 500 °C for 2 h. WGS was operated from 180 °C by intervals of 20 °C approximately every 1h30, at 3.0 ± 0.2 bar relative. Flows used were 20 mL/min of CO, 150 mL/min of Ar and 0.08 mL/min of liquid distilled water. This corresponds to a ratio S/C of 5.5 and a GHSV of 30,744 h^{-1}. In some experiments, water flow rate was additionally varied at 0.02, 0.04 and 0.30 mL/min resulting in S/C of 1.4, 2.8 and 20.7 and GHSV of 21,686, 24,705 and 63,959 h^{-1} respectively. Both gases and water were pre-heated at 180 °C before being introduced in the reactor. Dried permanent gases (CO, CO_2, H_2, CH_4) were analyzed every 5 min (30 min during the night) by online µ-GC/TCD (Agilent 990) connected after the reactor [39].

The biocarbon catalysts were characterized using various techniques, but only metal content for Ni and Fe (ICP), textural properties (BET, N_2) and surface chemical groups (TPD, TPR, TPO) are presented here. The changes in the structure of the biocarbon catalyst were analyzed before and after the chemical reaction.

Performance of the Biocarbon Catalysts

The performance of the biocarbon catalysts was estimated in terms of selectivity and conversion. Selectivity (S) facilitates the comparison of produced molecules and identify, in this case, if CO forms preferentially the main product CO_2 or the byproduct CH_4. Therefore, selectivity was defined as the ratio of the molar or volumetric flow ($\dot{V}$) of the target

Table 1 Summary of main elemental composition for the produced biocarbon catalysts

Catalyst	Biomass (fern, F)	Metal	Impregnation before (B)/ after (A) pyrolysis	Elemental analysis wt%					Ash content	Metal content wt% in catalyst	
				C	H	*N*	S	O (by difference with CHNS)	wt%	Fe	Ni
RF	F	–	–	72.78	0.93	1.47	< 0.01	24.82	14.4	0.03	< 0.01
FFe-B	F	Fe	B	71.01	0.49	1.07	< 0.01	27.43	28.1	13.17	< 0.01
FNiFe-A	F	Fe, Ni	A							0.36	0.76
FNi-B	F	Ni	B	71.23	0.73	1.86	< 0.01	26.18	20.4	< 0.01	3.96
FNi-A	F	Ni	A	75.72	1.14	1.65	< 0.01	21.49	13.7	< 0.01	1.43
FNiFe-B	F	Fe, Ni	B	66.99	0.84	1.15	< 0.01	31.02		8.08	10.30
FNi-A no red	F	Ni	A	75.72	1.14	1.65	< 0.01	21.49	13.7	< 0.01	1.43
Fe_2O_3 (> 97%)	–	Fe	–	Not applicable						67.85	< 0.01

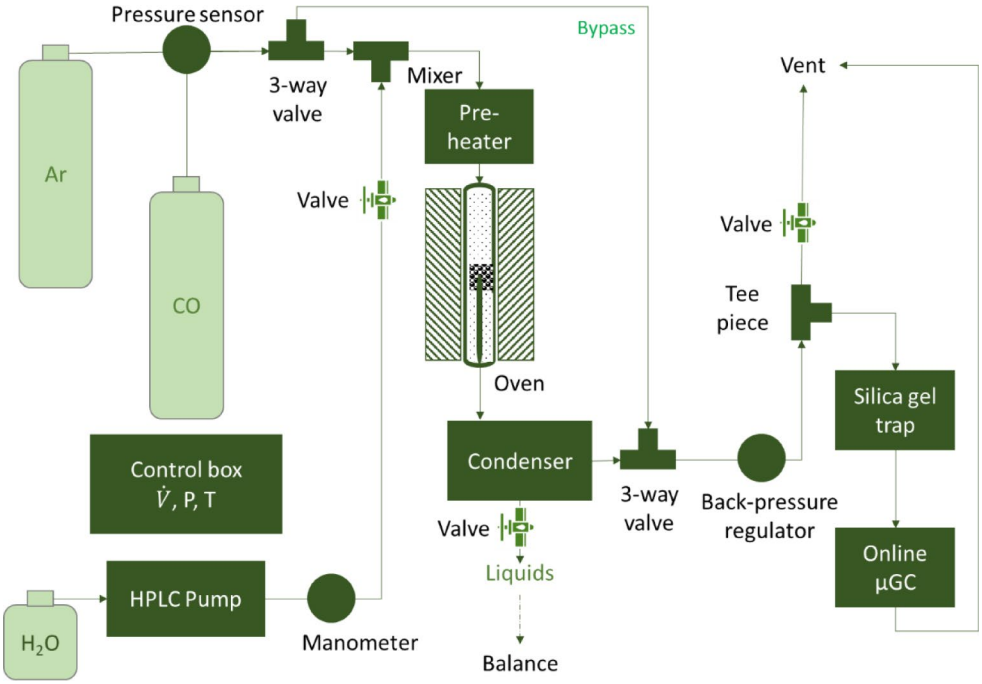

Fig. 1 Set-up for the water-gas shift (WGS) experiments

carbon gas produced compared to the sum of all carbon gases produced through the reaction Eqs. 5 and 6).

$$S_{CO_2} = \frac{\dot{V}_{CO_2}}{\dot{V}_{CO_2} + \dot{V}_{CH4}} \tag{5}$$

$$S_{CH_4} = 1 - S_{CO_2} \tag{6}$$

The conversion of the limiting gas represents the CO consumption to form products. A higher conversion represents a higher activity from the biocarbon catalyst. Conversion (X) was therefore defined as the ratio between the consumed amount of CO, calculated by the difference of inlet and outlet flow rate, divided by the inlet flow rate of the respective gas (Eq. 7).

$$X_{CO} = \frac{\dot{V}_{inlet,CO} - \dot{V}_{outlet,CO}}{\dot{V}_{inlet,CO}} \tag{7}$$

The rate of CO_2 production (r_{CO_2}) was determined according to the variation in CO_2 concentration multiplied by the total flow rate divided by catalyst mass. Therefore, it represents the flow of CO_2 produced over the catalyst (Eq. 8) [21].

$$r_{CO_2} = \frac{\Delta\, CO_2 \dot{V}_{total}}{m_{catalyst}} \tag{8}$$

Simulation, Test and Impact of the Variation of Temperature and Water Partial Pressure in WGS Reaction

Kinetic and Thermodynamic Simulations of WGS Reaction Conditions

In this section, the set-up for WGS and the selected operating conditions are optimized thanks to kinetic and thermodynamic simulations carried out on Aspen Plus. Initially, the pre-heating process was simulated to determine the required pre-heating temperature to limit condensation of water before the reactor, as too much liquid water could transport the catalyst downstream the oven. The influence of the pressure was also tested. The reaction atmosphere (argon), as well as reactive and produced gases were introduced as conventional components and the Peng Robinson – Boston Mathias (PR-BM) thermodynamic method was selected [40].

The Aspen flowsheet for pre-heating was defined by three blocks: a mixer and 2 heat exchangers. The 1st heat exchanger acts as the pre-heating temperature. It simultaneously defines the pressure before reaching the following blocks which are dependent on this pressure. The pressure of the experimental device is fixed by a back-pressure regulator located after the condenser that helps liquify condensable gases from the reactor and this regulator fixes the pressure preceding it (Fig. 1). The 2nd exchanger represents the heat loss before entering the reactor. The heat loss (Q_{loss}) was quantified by convective exchange of the exterior of the tubing (28 cm long, 14 mm diameter) between the

pre-heater and the reactor with ambient temperature (T_{amb}: 21 °C). A thermocouple was used to measure the temperature of the tube's exterior (T_{tube}) along its length: 80 °C for 2 cm, close to ambient for the rest of the tube. To account for overheating, possible loss of isolation around the tube and generally to overestimate the loss, half of the tube was considered at 80 °C. The convective heat transfer coefficient (h) was selected as 10 W m^{-2} K^{-1} (average value for natural convection) [41]. The heat loss in these conditions was estimated at 3.93 W (Eq. 9). Additionally, this worst-case scenario considered a liquid water flow rate of 1 mL/min. This liquid water is then vaporized in the pre-heating stage before being introduced in the reactor as steam.

$$Q_{loss} = h \times S \times (T_{tube} - T_{amb}) \tag{9}$$

180 °C was selected for pre-heating to have a safe interval to account for possible increase in pressure and possible drops in temperature. This is what happens for example when significantly increasing water flow to guarantee its delivery to the reactor.

Following the pre-established flowsheet, the WGS reaction was simultaneously assessed in 2 scenarios: kinetic-driven conditions using a plug flow reactor and thermodynamic-driven conditions using a Gibbs reactor followed by a condenser at 10 °C. Conditions for pre-heating were established as 0.58 W, corresponding to the estimated heat loss (2 cm of the tube at 80 °C), and 3 bar of relative pressure, as with experimental WGS. The plug flow reactor represents the stoichiometric conversion according to reaction kinetics. The Gibbs reactor calculates the composition at thermodynamic equilibrium of outlet gas based on the minimization of Gibbs energy of the selected components at specified temperature (varied) and pressure (isobaric) [3, 11].

The plug flow reactor block contains a specified reactor temperature (varied), dimensions set at 6 cm of length (estimate of catalyst bed length) and 8 mm of diameter, and a set of power law reactions to represent WGS and RWGS, and to introduce formation and consumption of CH_4 via methanation (MET) and steam methane reforming (SMR) respectively (Eqs. 2, 10 and 11) [42, 43]. These reactions were characterized by a specific set of parameters from the Arrhenius equation (Eq. 3, Table 2). For WGS, both constants are low relative to previously reported values (up to 5.8×10^{10} and 130 kJ/mol) and could result in similar results due to the compensative effect of both constants. The other reactions (RWGS, MET, SMR) have however more elevated constants which could result in them being less active in WGS conditions. SMR could be the most active due to lowest activation energy and highest kinetic constant of the 3. Inversely, RWGS could be the least active.

Table 2 Set of parameters to kinetically simulate WGS process [17, 20, 40, 44–48]

Reaction	k_0 (rate dependent unit)	E_a (kJ/mol)
WGS	5.4×10^4	67.1
RWGS	6.4×10^6	326.4
MET	2.8×10^{15}	243.9
SMR	1.2×10^{16}	240.1

$$CO_2 + H_2 \leftrightarrow CO + H_2O \tag{10}$$

$$CH_4 + H_2O \leftrightarrow CO + 3H_2 \tag{11}$$

A sensitivity analysis was performed on steam excess (S/C) and on the temperature of the selected reactor (T) to observe their influence on conversion, selectivity and outlet gas composition. S/C was observed from 1.4 to 20.7, with an incremental step of 1.4. T was varied from 180 °C (pre-heating temperature) to 400 °C (high temperature WGS) every 20 °C.

For the plug flow reactor, conversion, selectivity and generally gas composition were unaffected by increasing temperature. Conversion increased initially from 1.5 to 3.3% for a S/C from 1.4 to 8.3 then dropped to 2.7% at 20.7 (Supporting Information, Fig. S2). The increase in S/C results in less water being vaporized when reaching the reactor which may cause the conversion drop since the reactor cannot provide enough energy to produce steam while maintaining the reaction. With this given set of kinetic parameters, only WGS and RWGS are dominant, resulting in a CO_2 selectivity of 100%. The experimental gas composition takes into account the Ar as an inert sweeping gas and does not consider the water composition of water as it is condensed before arriving at the μGC. So, to imitate experimental conditions and facilitate further comparison, the simulated results were corrected by accounting for presence of Ar by adding it to the mix of reactive and produced gases, and by removing water content. The resulting simulated gas composition follows the same trend as conversion (Fig. 2) with H_2 and CO_2 reaching a maximum of 0.4% at 8.3. CO is consumed accordingly.

For the Gibbs reactor, conversion increased with increasing S/C and decreasing T. It was above 99% and is coherent with thermodynamic calculations and equilibrium principles [8]. Inversely, increasing S/C and T improves CO_2 selectivity and therefore lowers CH_4 selectivity (Supporting Information, Fig. S3). Values for S_{CO_2}, remain above 75%, meaning WGS is favored compared to methanation. This is exacerbated by the increase in $\dot{V}_{H_2O}$ that forces WGS towards the production of CO_2 and T that when increased favors the least exothermic reaction (WGS) between WGS and MET (Eqs. 1 and 2).

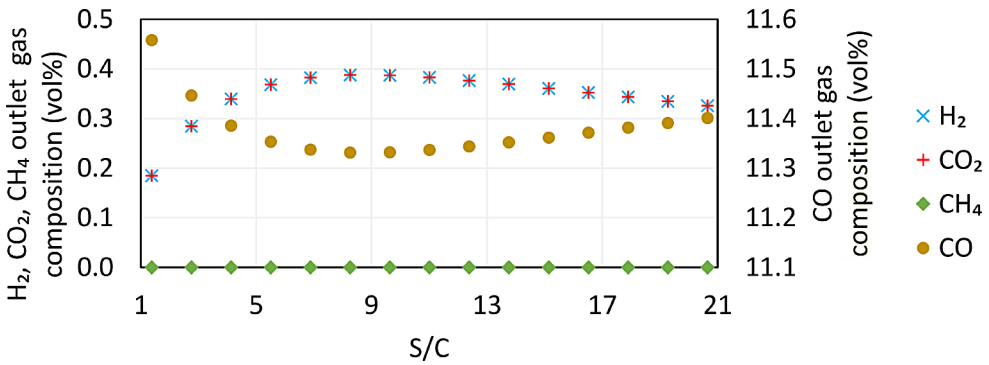

Fig. 2 Impact of variation in S/C on outlet gas composition in plug flow reactor (no effect from T)

Both scenarios tend to have opposite results, with conversion being either close to 100% when the reaction is thermodynamically driven or close to 0% when kinetically driven. The methanation reaction is also more or less dominant in terms of CO selectivity. Therefore, depending on experimental results, operating conditions and the catalytic effect of the studied catalysts, the reaction can be either kinetically driven, in which case the conversion should be low and selectivity high, or thermodynamically driven, where conversion is high and selectivity is impacted but still directed towards CO (> 75%). The corrected simulated gas composition will be summarized after presentation of these experimental results (Table 7).

WGS Reaction

Fern-based (F) biocarbon catalysts were tested in WGS to observe the influence of the impregnation type (before and after pyrolysis, B or A), the impregnated metal (Fe and Ni) and WGS operating conditions, namely temperature and water flow. They were also compared to rust (Fe_2O_3), and the influence of reduction on the fern biocarbon catalyst impregnated with Ni after pyrolysis was studied (FNi-A no red). It was reported to reach at most 20% CO conversion at 300 °C under comparable pressure, GHSV and S/C (5.5). This conversion is increased when the metal is promoted and supported (reaching 70%) [29, 49, 50].

Influence of the Temperature

The influence of the temperature was evaluated by the CO_2 production in WGS from 180 °C to at least 280 °C by increasing temperature in intervals of 20 °C approximately every 1h30 for nickel and iron biocarbon catalysts, as well as rust. The visualization of the impact of this increase in temperature (T), and the modification of steam excess (S/C) on gas production, is facilitated by the representation of the time-dependent evolution of CO_2 production (Fig. 3, Fig. S4 in Supporting Information). The experiment was repeated for the most active catalysts, which resulted in a relative standard deviation (RSD) of 9.6%. Also, the µGC can detect gases up to 0.001 vol%.

According to the results, Ni-based catalysts were shown to be more active, while rust was the least active. It showed the lowest activity with a maximum CO_2 concentration of 0.04 vol% at 360 °C (Fig. 3). When compared to simulated results and reported literature values (S/C = 3.5, GHSV = 60,000 h^{-1}, T = 400 °C), CO_2 concentration should be close to 2.2 vol%. This value was obtained as a result of a cross-multiplication between the maximal simulated CO_2 concentration (0.37 vol%, Fig. 2), the maximal reported CO conversion (20%) and the maximal simulated conversion (3.3%) [29, 50]. The CO_2 concentration obtained in this study reached 0.20 vol%, so the 11-fold difference in experimental and reported values could be related to a difference in unmentioned operating conditions (pressure, presence of inert gas, bed size). The quantity of produced CO_2 (max. 0.20 vol%) compared to that of the simulated results (kinetic: 0.37 vol%) shows the kinetically driven nature of WGS in our conditions. The limitations associated with these conditions are therefore an important factor linked with these low values. This is however accompanied by stronger kinetic properties on behalf of the biocarbon catalysts that outperformed rust. Additionally, the observation of the temporal evolution of CO_2 concentration (Fig. 3) seems to indicate a deactivation of the catalysts (decrease in value over time) that is steeper as the temperature is increased. The decrease may be linked to active site sintering or reactant surface saturation [51–54].

To compare the performances of biocarbon catalysts, the maximum CO_2 production reached at each temperature was represented, as well as CO conversion and CO_2 selectivity (Table 3). Additionally, maximum H_2 production was observed (Supporting Information, Table S2).

Under 240 °C, the activity of FNi-A (reduced or not), FNiFe-B and FNi-B appears to be slightly higher. This points out a low temperature activity that might be related to the presence of Ni. At low temperatures, the catalysts and WGS are unstable due to activation energies required from both catalyst and reacting gases. Additionally, little gas is

Table 3 Impact of reactor temperature on peak CO_2 production, CO conversion and CO_2 selectivity of biocarbon catalysts and rust

	T (°C)	Rust	FFe-B	RF	FNiFe-A	FNi-A no red	FNi-B	FNi-A	FNiFe-B
CO_2 outlet gas composition (vol%)	180	0.007	0.008	0.001	0.006	0.003	0.012	0.047	0.013
	200	0.004	0.004	0.005	0.008	0.029	0.010	0.028	0.022
	220	0.004	0.005	0.006	0.009	0.019	0.015	0.046	0.041
	240	0.005	0.007	0.008	0.013	0.021	0.026	0.069	0.076
	260	0.006	0.010	0.011	0.018	0.028	0.046	0.102	0.128
	280	0.008	0.015	0.015	0.027	0.041	0.090	0.136	0.204
CO conversion (%)	180	6.4	8.2	7.2	8.4	8.4	8.1	8.3	8.4
	200	6.7	8.3	7.0	8.3	7.6	7.9	8.3	8.0
	220	6.7	8.0	6.9	8.2	8.2	7.9	8.4	8.4
	240	6.6	8.0	7.1	8.4	8.2	8.1	8.9	8.6
	260	6.6	7.9	7.0	8.4	8.2	8.5	9.0	9.5
	280	6.9	7.9	7.0	8.5	8.5	9.0	9.6	10.3
CO_2 selectivity (%)	180	100.0	100.0	22.6	96.7	100.0	100.0	100.0	100.0
	200	100.0	93.8	84.6	95.8	100.0	95.8	97.3	100.0
	220	96.0	98.1	100.0	92.1	89.6	92.3	92.6	100.0
	240	100.0	100.0	98.2	92.2	90.0	86.8	94.8	100.0
	260	97.0	88.9	100.0	100.0	95.8	93.7	95.1	100.0
	280	100.0	100.0	96.7	100.0	97.3	94.3	98.5	99.7

formed and are close in composition to the μGC detection limit, resulting in selectivity and CO_2 composition highly reliant on the catalytic activity. The active site sensibility and electronic activity could be related to the ability to reversibly transform from an oxidized to a reduced state allowing activity in WGS. This is supported by TPR results where weaker reducible sites are represented by low peak temperature (as low as 355 °C for FNi-A) and the quantity of these sites is represented by the amount of H_2 desorbed [29, 55–57] In this study, the biocarbon catalysts were reduced at 500 °C which could justify higher activity from FNi-A and FNiFe-B (lowest H_2 peak at 514 °C). This could also be correlated with the ability to easily adsorb CO or steam where Ni-based catalysts showed stronger adsorptive capacities for NH_3 and CO_2 respectively (Table 4, Fig. S5–S7 in Supporting Information) of at least 0.8 and 12.0 mmol/g respectively for Ni-based catalysts compared to 0.6 and 8.3 mmol/g for FFe-B. This is further amplified as Ni-based biocarbon catalysts present a higher amount of reducible sites, of at least 1.0 mmol/g for Ni compared to 0.2 for FFe-B. Once reduced, these sites are sources of O vacancies that complement and facilitate the adsorption and reactivity of O from CO and steam.

Above 240 °C, the catalytic activity in relation to the CO_2 production increases by approximately 50% according to the following order: rust < FFe-B < RF < FNiFe-A < FNi-A not pre-reduced (no red) < FNi-B < FNi-A < FNiFe-B. There are similar trends for lower temperatures: Ni catalysts are generally more active for WGS which could be related to their lower activation energies [58, 59]. This activity might be further amplified when considering the presence of other metals with promoting and supporting effects (alkali and alkaline earth metals, Co, Cu, Zn, Al, …) that help reduce even further energy barriers. The individual effect of inherent metals, impregnation type and metal and resource type, on WGS, is hard to determine as metal content varies between samples (Table 1). The performance of FNi-A could be improved through reduction as the CO_2 production of the pre-reduced FNi-A is 3 times higher than that of its not pre-reduced counterpart. This can be expected because through reduction the biocarbon catalyst gains O vacancies which act as reaction sites for both steam and CO. The formation of Ni nanoparticles that further enhance the WGS activity is also facilitated through this process [60–62]. On another hand, impregnation and pyrolysis could induce a loss of activity and specific surface area due to blocking of the access to pores containing active sites, induced by in-solution metals and carbon deposit respectively [63, 64]. Here, pores and especially active sites are exposed as the specific surface area increases (Table 4) but the unhindered metals maintain their respective activities (Tables 3 and 5) that are unaffected by this increase in surface area. The high

Table 4 Chemical surface groups versus specific surface area of the biocarbon catalysts before WGS

Sample	TPD-NH_3		TPD-CO_2		TPD-H_2		Specific surface area (m^2/g)
	Total adsorption (mmol/g)	T_{max} (°C)	Total adsorption (mmol/g)	T_{max} (°C)	Total adsorption (mmol/g)	T_{max} (°C)	
RF	0.8	913	12.0	915	2.5	993	8.8
FFe-B	0.6	951	8.3	905	0.2	981	309.6
FNi-B	1.5	912	16.2	920	2.9	986	151.6
FNi-A	0.8	945	12.0	923	1.7	989	100.0
FNiFe-B	1.1	923	16.0	924	1.0	1000	367.9

Table 5 Impact of steam excess on peak production of CO_2, CO conversion and CO_2 selectivity of biocarbon catalyst

S/C	CO_2 outlet gas composition (vol%)		CO conversion (%)		CO_2 selectivity (%)	
	RF (360 °C)	FNi-A no red (280 °C)	RF (360 °C)	FNi-A no red (280 °C)	RF (360 °C)	FNi-A no red (280 °C)
1.4	0.039		7.4		99.1	
2.8		0.031		8.0		100.0
5.5	0.048	0.038	7.6	8.4	100.0	98.7
20.7	0.056	0.041	7.7	8.5	98.3	97.3

Table 6 Estimated kinetic parameters for biocarbon catalysts and rust in pre-established decreasing order of performance

Catalyst	E_a (kJ/mol)	$k_{0,\ biocarbon\ catalyst}/k_{0,\ rust}$
FNiFe-B	59.5	$5.6\times10^5 = e^{11.6}$
FNi-A	26.8	$1.8\times10^2 = e^{5.8}$
FNi-B	92.1	$2.2\times10^8 = e^{19.2}$
FNi-A not pre-reduced	22.1	$1.4\times10^1 = e^{2.7}$
FNiFe-A	43.3	$1.3\times10^3 = e^{7.2}$
RF	7.5	$3.9\times10^{-1} = e^{-1.0}$
FFe-B	5.2	$2.2\times10^{-1} = e^{-1.5}$
Rust	9.5	$1 = e^0$

surface developed by Fe-based biocarbon catalysts, possibly related to catalyzed graphitization, does not therefore benefit its activity [65, 66]. The degree of metal exposition and activity, and carbon graphitization may also vary depending on the metal content of each sample. These aspects have been discussed in a previous study on RWGS, through X-ray diffraction and high-resolution transmission electron microscopy techniques [33]. Additionally, the specific surface area of the catalysts after WGS was analyzed (Supporting Information, Table S3). An increase in specific surface area may be observed but could also be a result of mixing with alumina. X-ray diffractograms for FNi-B before WGS seem to indicate reduced Ni sites and may indicate possible graphitization as C is used to reduce Ni during pyrolysis (inert atmosphere) (Fig. S8).

CO conversion reached 10.3% at 280 °C using FNiFe-B. The highest increase due to temperature was with this same catalyst and was 1.9% from 180 to 280 °C (Table 3). Additionally, rust, RF and Fe-based biocarbon catalysts (except FNiFe-B) converted less (< 8.5%) and were slightly influenced by temperature as the increase in conversion due to the temperature was at most 0.3%. This could again be related to the facilitated reducibility of Ni-based catalysts (Table 3). Due to the reaction being kinetically driven, an increase in temperature improves conversion until the reaction reaches thermodynamic equilibrium (99%) [19, 28, 29, 31, 67, 68]. As mentioned previously, in studies with similar operating conditions, rust can reach up to 20% conversion but reached at most 6.9% in this study, and is indicative of severe kinetic limitations [29, 49, 50]. It also reflects the compatibility of the biocarbon catalysts for WGS reaction [69]. Additionally, the biocarbon catalysts outperformed rust, possibly due to rust bulk not benefitting from enhanced activity towards WGS through dispersion of nanosized active sites [70]. The biomass inherent metals may also enhance the electronic state of reactive metals and improve their activity at lower temperatures [71].

Selectivity towards CO_2 was globally above 85% and nearing 100% when performing the reaction at high temperatures (> 240 °C) with active catalysts (Table 3). This proved that the conditions were favorable to inhibit the methanation reaction (Eq. 2) that produces CH_4. As previously mentioned, methanation is more exothermic than WGS thus increasing temperature should lessen the formation of CH_4 [20]. Methanation is also reported to have higher activation energies (243.9 kJ/mol, Table 2) than WGS (67.1 kJ/mol) and could suffer more severe kinetic limitations.

Influence of the Steam Excess

S/C was varied between 1.4 and 20.7. This variation was carried out at the end of the experiment for RF (360 °C) and FNi-A not pre-reduced (280 °C, Table 5).

It was observed that the production of CO_2 increased by approximately 0.007 vol% with each increase in S/C. This is coherent with the literature as an increase in S/C shifts WGS

Table 7 Summary of averaged values of concentrations, selectivity and conversion for biocarbon catalysts

Conditions: 280 °C, S/C = 5.5				Outlet gas composition (vol%)				Conversion (%)	Selectivity (%)	
Biocarbon catalysts and rust			Initial composition	CO	CO_2	H_2	CH_4	X_{CO}	S_{CO_2}	S_{CH_4}
				11.76	–	–	–	–	–	–
			WGS kinetic simulation							
				11.35	0.37	0.37	< 0.00	3.1	100	< 0.0
Sample	Biomass	Metal	Impregnation before/after pyrolysis	Outlet gas composition (vol%)				Conversion (%)	Selectivity (%)	
			Metal content (wt% in biocarbon)	CO	CO_2	H_2	CH_4	X_{CO}	S_{CO_2}	S_{CH_4}
RF	Fem	–	–	9.70	0.01	0.01	< 0.00	7.0	96.7	3.3
FFe-B	Fem	Fe	Before	9.69	0.01	0.02	< 0.00	7.9	100	< 0.0
			13.17							
FNiFe-A	Fem	Fe, Ni	After	9.63	0.02	0.03	< 0.00	8.5	100	< 0.0
			0.76,0.36							
FNi-B	Fem	Ni	Before	9.57	0.08	0.09	0.01	9.0	94.3	5.7
			3.96							
FNi-A	Fem	Ni	After	9.52	0.12	0.14	< 0.00	9.6	98.5	1.5
			1.43							
FNiFe-B	Fem	Fe, Ni	Before	9.46	0.17	0.21	< 0.00	10.3	99.7	0.3
			10.30,8.08							
FNi-A no red	Fem	Ni	After	9.64	0.04	0.04	< 0.00	8.5	97.3	2.7
			1.43							
Fe_2O_3	–	Fe	–	9.67	0.01	0.01	< 0.00	6.9	100	< 0.0

towards the production of CO_2 and H_2 due to the excess of one reactant (steam in this case) and the resulting displacement in equilibrium. This increase continues at higher values of S/C (> 10) but the increase then lessens above 10 [18, 19, 30, 31, 53, 72].

The increase in S/C seemed to slightly increase the conversion (by 2.5%< RSD) which could be caused by the equilibrium displacement but the effect of this increase is neglectable. A peak of CO_2 production and therefore CO conversion should be observed at S/C = 8.3 based on the simulated kinetic results (Fig. 2, 0.4 vol% and 3.3% respectively). This was not the case with the experimental results since the increase continued when increasing S/C from 5.5 to 20.7 (Table 5). This increase is also however slight, from 0.003 to 0.008 vol% for CO_2 production and 0.1% for CO conversion, and in error ranges.

According to the literature, an increase in flow rate reduces contact time allowing formation of CH_4 and an increase in S/C drives the consumption of CH_4 through SMR [73–75]. Therefore, CO_2 selectivity should improve with excess steam and high GHSV. In our case, the increased reactant excess did not show an influence on the selectivity. However, selectivity was close to 100% which is comparable to the simulated kinetic results (Fig. 2).

Kinetic Parameters

Kinetic parameters were estimated via power law and Arrhenius equations (Eqs. 3 and 8). By assuming nearly constant partial pressures and high CO selectivity, equations were obtained (Eqs. 12–13) and kinetic parameters were deduced (Table 6) [67].

$$\ln\left(r_{CO_2}\right) = -\frac{E_a}{RT} + \ln\left(k_0\right) + constant \tag{12}$$

$$\frac{k_{0,\,biosourced\,catalyst}}{k_{0,rust}} = e^{\ln\left(r_{CO_2,biosourced\,catalyst}\right) - \ln\left(r_{CO_2,rust}\right)} \tag{13}$$

The most performant catalysts present relatively high kinetic constants, which is beneficial for kinetic-driven WGS, but also present high activation energy. This phenomenon is reversed for the least performing catalysts and indicates the importance of the dual effect from both parameters. No immediate conclusion can be drawn based on a comparative factor accounting for the contribution of both parameters (such as comparing rates). However, this underlines the importance of the intrinsic characteristics of the biocarbon catalysts that have no immediate catalytic impact (thermal, electric and electronic conductivity). Regardless, the experimental values obtained for the activation energy and the pre-exponential factor, compared to literature, are

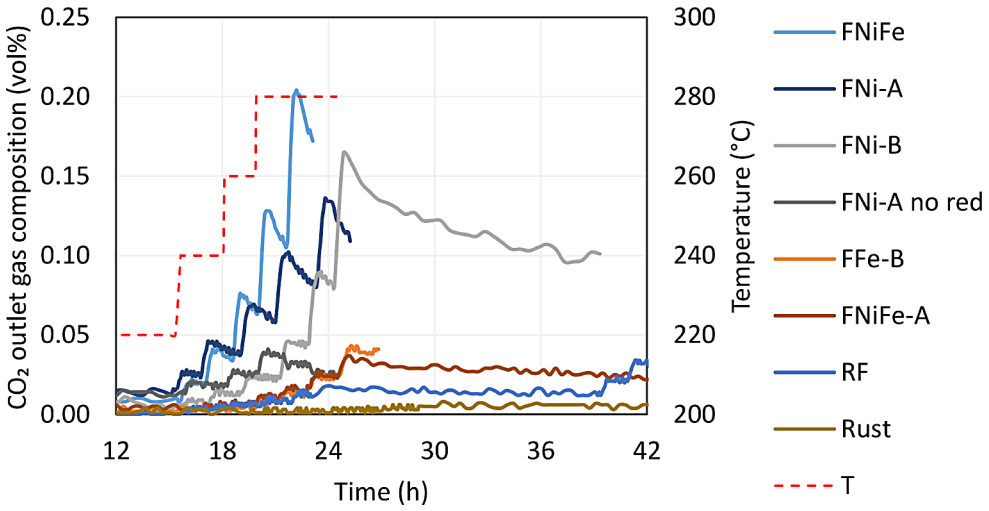

Fig. 3 Evolution in time of CO_2 production by catalyzed WGS, T varied

of the same order of magnitude [17, 21, 22]. Furthermore, the assumptions to obtain these parameters are insufficient to completely describe the rate law. For example, the orders for each reactant and product were not determined. Indeed, CO formation rates are highly dependent on the partial pressures of formed gases and their respective orders, and do not consider possible methane production (Eq. 3) [15–18, 21, 32, 34, 42, 43].

Summary of the Reaction Performances

The performance of the biocarbon catalysts was evaluated in WGS reaction through CO conversion and selectivity towards CO_2 and CH_4. The results obtained at 280 °C and S/C = 5.5, in terms of concentration of reactive gases (CO) and product gases (CO_2, H_2 and CH_4) were indicated (Table 7) to facilitate comparison and hierarchy of the biocarbon catalysts performance. This temperature is the highest studied for all catalysts and for which the CO_2 production and CO conversion are sufficiently high to allow a more precise comparison. The biocarbon catalysts (not rust nor FNi-A no red) were ordered by increasing conversion (Table 7).

To summarize, CO_2 and H_2 gas production and inversely CO consumption is higher with Ni-biocarbon catalysts than with Fe-biocarbon catalysts or rust. The most performant catalyst FNiFe-B combines the properties of both metals. Ni-based catalysts in particular are functional for low temperature WGS as they can alternate between reduced and oxidized states at low temperatures with little energy [29, 55–57]. CO conversion is improved as CO consumption is increased and follows this same tendency. CO_2 selectivity decreases as CH_4 production increases. This is mostly the case with Ni-based biocarbon catalysts but CO_2 selectivity in this instance is above 94%.

The highest experimental gas production is 0.17 vol% for CO_2 and 0.21 vol% for H_2, while a maximum of 0.37 vol% was obtained through simulations for both gases. These values need to be considered by taking into account that µGC sensitivity is 0.001 vol% and RSD is 10%. The difference in gas production could be due to lower WGS activity as the kinetic parameters used in the simulation (Table 2) are based on highly efficient and optimized catalysts such as Pt-based catalysts [17, 20, 40, 44–48]. Additionally, it is possible that some gas is adsorbed by the biocarbon and the moisture trap [76]. CO conversion by the biocarbon catalysts is at least 6.9%, which is higher than the maximal simulated conversion (3.1%). The difference in simulated and experimental conversions could be related to lower values of experimental CO concentration (11.35 compared to 9.70 vol% respectively). Since the experimental value is lower, the variation of this concentration will be more important, which will result in higher conversion (Eq. 7). Even if experimental conversion values may appear as low (< 10%), similar reported trends have been observed: Ni-based catalysts were more active at lower temperatures than Fe-based catalysts [69]. This conversion can be improved further by changing the kinetic parameters (catalyst) and displacing equilibrium through increase of temperature and steam excess (operating conditions). This increase in temperature will however be limited by thermodynamic equilibrium (Fig. 3) that diminishes as temperature increases, in addition to the loss of catalyst stability in relation to sintering. Also, the impact of excess steam stagnates as it is increased and even decreases WGS activity based on simulations (Fig. 2) [30, 31, 68]. The comparison between the obtained results for WGS simulation and experiments was summarized (Table 8).

These results differ from previously studied RWGS where the reaction was partially thermodynamically-driven (namely at 400 °C). In this work, rust was the most active

Table 8 Synthesis of the comparison between the obtained results for WGS simulation and experiments

Parameters	Result	Discussion
Simulated plug flow reactor	Kinetic simulations result in low conversion (< 3.3%) with maximal conversion reached at specific value of steam excess and nearly 100% selectivity; no impact from T	The simulations are regulated by the set of kinetic parameters and resulted in WGS dominance (high selectivity) at a cost to activity (poor activity); high steam excess (> 8.3) does not benefit WGS activity as energy for the reaction is diverted to steam
Simulated Gibbs reactor	Thermodynamic simulations tend towards high conversion (> 99%) and selectivity (> 75%)	Conversion increases with excess steam but decreases with temperature and inversely for selectivity: equilibrium principles and exacerbation of CH_4 producing reactions (more exothermic than WGS) by steam
T	• Biocarbon catalysts are more active than rust and when reduced • Ni-based biocarbon catalysts are more active especially at lower T • 11-fold difference between experiments and literature • Instability below 240 °C • Increase in conversion and high selectivity	• O vacancies caused by reduction of O-containing biocarbon surface groups could improve CO and steam uptake and reactivity; other inorganic element namely AAEM and co-catalytic metals may help reduce energy barriers • Ni may be active and accessible at low T thanks to low T reversibility and to sufficiently developed porosity • Difference between this study and others could be related to operating conditions not addressed here • Instability may be related to electronic sensitivity and competition between activation of catalysts and reacting gases • Increasing T enhances kinetics, increases CO consumption and inhibits methanation that is more exothermic than WGS
S/C	• Increase of CO_2 production • Increase in conversion even at higher S/C values (20.7) • Little influence of selectivity but close to 100%	• Displacement of equilibrium towards the products of WGS due to excess of steam • Contradiction with simulation as maximum performance observed at 8.3 S/C but coherent with displacement of equilibrium • Coherent with simulation, excess steam that promotes CH_4 reforming and increase in GHSV that limits time to form CH_4
Kinetic (global)	• The reaction is kinetically driven with high conversion (< 10%) and selectivity (> 85%) • Biocarbon catalysts outperformed rust	• Inherent metals, facilitated reducibility and O vacancies could improve biocarbon performance but a change in operating conditions could enable thermodynamic equilibrium • $E_a = 5.2$ kJ/mol and and $k_0/k_{0,\,rust} = 2.2 \times 10^8$ for biocarbon catalysts compared to 9.5 kJ/mol and 1 for rust, respectively: high kinetic performance observed at low T (< 400 °C) for biocarbon catalysts in WGS
Influential parameters	The impact of T and S/C on CO conversion and CO_2 and CH_4 selectivity was tested over Fe and Ni-impregnated fern-based catalysts	The most influential parameters were T, CO conversion and Ni-based catalysts as WGS was driven by kinetics and catalytic activity improved with both T and Ni-based catalysts S/C influence was in range of errors and selectivity was high since methanation was not favorable in the studied operating conditions

but least stable catalyst whereas biocarbon catalysts performed well since high conversions were maintained for the duration of the experiment (72 h) and the catalyst did not suffer deactivation. The most active catalysts were fern-based catalysts which contained both Fe and Ni. Their activity was related to the synergetic effect of inherent metals with O vacancies resulting in improved electronic properties. In the case of WGS, inherent metals allow minimal activity but are confronted to energy barriers that limit their activity. Therefore, while Ni has strong electronic properties and low-temperature reducibility, which can react easily in restricting operating conditions (low temperature), Fe does not present such properties and will be limited when performing WGS. In both RWGS and WGS, biocarbon catalysts possessed homogenous inherent metals and available active and adsorptive sites that resulted in high performance, stability and selectivity. Further modifications to these properties may help to improve their performance respective to the tested reaction.

Conclusion and Perspectives

Biocarbon catalysts from fern were tested in original WGS conditions with increments in temperatures ranging from 180 to 400 °C and in S/CO from 1.4 to 20.7, every 1h30.

Results showed that WGS is kinetically-driven: conversion increased as temperature increased. Biocarbon catalysts outperformed rust, which shows promising results compared to metallic catalysts. Ni-based biocarbon catalysts showed the best activity. This could be attributed to their low temperature activation. This is especially the case of the fern catalyst impregnated with Ni and Fe before pyrolysis, which resulted in a conversion above 10%. CO conversion and consequently CO_2 and H_2 gas production increased with S/CO ratio due to improved kinetics and displacement of equilibrium, respectively. Selectivity towards WGS was above 85% and was slightly affected by temperature and S/CO, where their increase inhibits the side reaction producing CH_4. Kinetic parameters were determined for the biocarbon catalysts relative to rust and are comparable to literature values. No explicit relation between the order of the biocarbon catalysts' activity and these parameters was established. Characteristics with subtle impact on the kinetics may therefore need to be brought to light. Future work should observe these characteristics and optimize operating conditions to direct WGS towards thermodynamic equilibrium, as well as analyze the impact of biocarbon catalysts on other environmental applications.

Supplementary Information The online version contains supplementary material available at https://doi.org/10.1007/s12649-024-02673-3.

Acknowledgements The authors sincerely acknowledge the support provided by Eizhy, which provided shrubland biomass used in this study, as well as the European Union's Horizon 2020 research and innovation program under grant agreement No 637020 – MOBILE FLIP for the willow biomass used in this study.

Authors' contributions **T. Graul**: Methodology, Formal analysis, Investigation, Writing – Original Draft, Visualization. **M. González Martínez**: Validation, Resources, Writing – Review & Editing, Visualization, Supervision, Project administration, Funding acquisition. **A. Nzihou**: Conceptualization, Validation, Resources, Writing – Review & Editing, Supervision, Project administration, Funding acquisition.

Funding This work was supported by Institut Mines-Télécom.

Data Availability The datasets generated during and/or analysed during the current study are available from the corresponding author on reasonable request.

Declarations

Conflict of Interest The authors declare no conflict of interest.

References

1. About, I.P.C.C.: https://www.ipcc.ch/about/
2. Pal, D.B., Chand, R., Upadhyay, S.N., Mishra, P.K.: Performance of water gas shift reaction catalysts: a review. Renew. Sustain. Energy Rev. **93**, 549–565 (2018). https://doi.org/10.1016/j.rser.2018.05.003
3. Chen, W.-H., Chen, C.-Y.: Water gas shift reaction for hydrogen production and carbon dioxide capture: a review. Appl. Energy. **258**, 114078 (2020). https://doi.org/10.1016/j.apenergy.2019.114078
4. Ratnasamy, C., Wagner, J.P.: Water gas shift catalysis. Catal. Rev. **51**, 325–440 (2009). https://doi.org/10.1080/01614940903048661
5. Shen, Y.: Chars as carbonaceous adsorbents/catalysts for tar elimination during biomass pyrolysis or gasification. Renew. Sustain. Energy Rev. **43**, 281–295 (2015). https://doi.org/10.1016/j.rser.2014.11.061
6. Wang, G., Jiang, L., Zhou, Y., Cai, Z., Pan, Y., Zhao, X., Li, Y., Sun, Y., Zhong, B., Pang, X., Huang, W., Xie, K.: Investigation of the kinetic properties for the forward and reverse WGS reaction by energetic analysis. J. Mol. Struct. (Thoechem). **634**, 23–30 (2003). https://doi.org/10.1016/S0166-1280(03)00209-4
7. Plata, J.J., Graciani, J., Evans, J., Rodriguez, J.A., Sanz, J.F.: Cu deposited on CeOx-Modified TiO2(110): Synergistic effects at the metal–oxide interface and the mechanism of the WGS reaction. ACS Catal. **6**, 4608–4615 (2016). https://doi.org/10.1021/acscatal.6b00948
8. Er-rbib, H., Bouallou, C.: Modeling and simulation of CO methanation process for renewable electricity storage. Energy. **75**, 81–88 (2014). https://doi.org/10.1016/j.energy.2014.05.115
9. Butterman, H.C., Castaldi, M.J.: Influence of CO2 injection on biomass gasification. Ind. Eng. Chem. Res. **46**, 8875–8886 (2007). https://doi.org/10.1021/ie071160n
10. Lambert, M., Leven, B.A., Green, R.M.: New methods of cleaning up heavy metal in soils and water. Env. Sci. Technol. Briefs Cirizens. **3**
11. Said, M., Cassayre, L., Dirion, J.-L., Joulia, X., Nzihou, A.: Effect of nickel impregnation on wood gasification mechanism. Waste Biomass Valor. **8**, 2843–2852 (2017). https://doi.org/10.1007/s12649-017-9911-3
12. Pahija, E., Panaritis, C., Gusarov, S., Shadbahr, J., Bensebaa, F., Patience, G., Boffito, D.C.: Experimental and computational synergistic design of Cu and Fe catalysts for the reverse water–gas shift: a review. ACS Catal. **12**, 6887–6905 (2022). https://doi.org/10.1021/acscatal.2c01099
13. Lèbre, É., Stringer, M., Svobodova, K., Owen, J.R., Kemp, D., Côte, C., Arratia-Solar, A., Valenta, R.K.: The social and environmental complexities of extracting energy transition metals. Nat. Commun. **11**, 4823 (2020). https://doi.org/10.1038/s41467-020-18661-9
14. Yuan, X., Cao, Y., Li, J., Patel, A.K., Dong, C.-D., Jin, X., Gu, C., Yip, A.C.K., Tsang, D.C.W., Ok, Y.S.: Recent advancements and challenges in emerging applications of biochar-based catalysts. Biotechnol. Adv. **67**, 108181 (2023). https://doi.org/10.1016/j.biotechadv.2023.108181
15. Ayastuy, J.L., Gutiérrez-Ortiz, M.A., González-Marcos, J.A., Aranzabal, A., González-Velasco, J.R.: Kinetics of the low-temperature WGS reaction over a CuO/ZnO/Al2O3 catalyst. Ind. Eng. Chem. Res. **44**, 41–50 (2005). https://doi.org/10.1021/ie049886w
16. Zhu, M., Wachs, I.E.: Iron-based catalysts for the high-temperature water–gas shift (HT-WGS) reaction: a review. ACS Catal. **6**, 722–732 (2016). https://doi.org/10.1021/acscatal.5b02594
17. Saeidi, S., Fazlollahi, F., Najari, S., Iranshahi, D., Klemeš, J.J., Baxter, L.L.: Hydrogen production: Perspectives, separation with special emphasis on kinetics of WGS reaction: a state-of-the-art review. J. Ind. Eng. Chem. **49**, 1–25 (2017). https://doi.org/10.1016/j.jiec.2016.12.003
18. Gosiewski, K., Tańczyk, M.: Applicability of membrane reactor for WGS coal derived gas processing: simulation-based analysis.

Catal. Today. **176**, 373–382 (2011). https://doi.org/10.1016/j.cattod.2010.11.042
19. Cornaglia, L., Múnera, J., Lombardo, E.: Recent advances in catalysts, palladium alloys and high temperature WGS membrane reactors: a review. Int. J. Hydrog. Energy. **40**, 3423–3437 (2015). https://doi.org/10.1016/j.ijhydene.2014.10.091
20. Angeli, S.D., Monteleone, G., Giaconia, A., Lemonidou, A.A.: State-of-the-art catalysts for CH4 steam reforming at low temperature. Int. J. Hydrog. Energy. **39**, 1979–1997 (2014). https://doi.org/10.1016/j.ijhydene.2013.12.001
21. Yan, H., Qin, X.-T., Yin, Y., Teng, Y.-F., Jin, Z., Jia, C.-J.: Promoted Cu-Fe3O4 catalysts for low-temperature water gas shift reaction: optimization of Cu content. Appl. Catal. B. **226**, 182–193 (2018). https://doi.org/10.1016/j.apcatb.2017.12.050
22. Mendes, D., Mendes, A., Madeira, L.M., Iulianelli, A., Sousa, J.M., Basile, A.: The water-gas shift reaction: From conventional catalytic systems to Pd-based membrane reactors—a review. Asia-Pac. J. Chem. Eng. **5**, 111–137 (2010). https://doi.org/10.1002/apj.364
23. Van der Laan, G.P., Beenackers, A.A.C.M.: Kinetics and selectivity of the Fischer–Tropsch synthesis: a literature review. Catal. Rev. **41**, 255–318 (1999). https://doi.org/10.1081/CR-100101170
24. Ghanekar, P., Kubal, J., Cui, Y., Mitchell, G., Delgass, W.N., Ribeiro, F., Greeley, J.: Catalysis at metal/oxide interfaces: density functional theory and microkinetic modeling of water gas shift at Pt/MgO boundaries. Top. Catal. **63**, 673–687 (2020). https://doi.org/10.1007/s11244-020-01257-4
25. Ding, K., Gulec, A., Johnson, A.M., Schweitzer, N.M., Stucky, G.D., Marks, L.D., Stair, P.C.: Identification of active sites in CO oxidation and water-gas shift over supported pt catalysts. Science. **350**, 189–192 (2015). https://doi.org/10.1126/science.aac6368
26. Majima, T., Kono, E., Ogo, S., Sekine, Y.: Pre-reduction and K loading effects on noble metal free co-system catalyst for water gas shift reaction. Appl. Catal. A. **523**, 92–96 (2016). https://doi.org/10.1016/j.apcata.2016.05.025
27. Patlolla, A., Carino, E.V., Ehrlich, S.N., Stavitski, E., Frenkel, A.I.: Application of operando XAS, XRD, and Raman spectroscopy for phase speciation in water gas shift reaction catalysts. ACS Catal. **2**, 2216–2223 (2012). https://doi.org/10.1021/cs300414c
28. Pastor-Pérez, L., Gu, S., Sepúlveda-Escribano, A., Reina, T.R.: Bimetallic Cu–Ni catalysts for the WGS reaction – Cooperative or uncooperative effect? Int. J. Hydrog. Energy. **44**, 4011–4019 (2019). https://doi.org/10.1016/j.ijhydene.2018.12.127
29. Khan, A., Smirniotis, P.G.: Relationship between temperature-programmed reduction profile and activity of modified ferrite-based catalysts for WGS reaction. J. Mol. Catal. A: Chem. **280**, 43–51 (2008). https://doi.org/10.1016/j.molcata.2007.10.022
30. Daly, H., Goguet, A., Hardacre, C., Meunier, F.C., Pilasombat, R., Thompsett, D.: The effect of reaction conditions on the stability of Au/CeZrO4 catalysts in the low-temperature water–gas shift reaction. J. Catal. **273**, 257–265 (2010). https://doi.org/10.1016/j.jcat.2010.05.021
31. Park, Y.M., Son, M., Park, M.-J., Bae, J.W.: Effects of pt precursors on Pt/CeO2 to water-gas shift (WGS) reaction activity with Langmuir-Hinshelwood model-based kinetics. Int. J. Hydrog. Energy. **45**, 26953–26966 (2020). https://doi.org/10.1016/j.ijhydene.2020.06.296
32. Palma, V., Pisano, D., Martino, M.: CFD modeling of the influence of carrier thermal conductivity for structured catalysts in the WGS reaction. Chem. Eng. Sci. **178**, 1–11 (2018). https://doi.org/10.1016/j.ces.2017.12.035
33. Graul, T., Gonzalez Martinez, M., Nzihou, A.: Nickel and iron-doped biocarbon catalysts for reverse water-gas shift reaction. ChemCatChem n/a, e202301398. https://doi.org/10.1002/cctc.202301398
34. Ghasemzadeh, K., Zeynali, R., Basile, A.: Theoretical study of hydrogen production using inorganic membrane reactors during WGS reaction. Int. J. Hydrog. Energy. **41**, 8696–8705 (2016). https://doi.org/10.1016/j.ijhydene.2015.12.117
35. Cheula, R., Maestri, M.: Nature and identity of the active site via structure-dependent microkinetic modeling: An application to WGS and reverse WGS reactions on Rh. Catal. Today. **387**, 159–171 (2022). https://doi.org/10.1016/j.cattod.2021.05.016
36. Munirathinam, R., Pham Minh, D., Nzihou, A.: Effect of the support and its surface modifications in Cobalt-Based Fischer–Tropsch synthesis. Ind. Eng. Chem. Res. **57**, 16137–16161 (2018). https://doi.org/10.1021/acs.iecr.8b03850
37. Lee, J.S., Kim, H.S., Park, N.-K., Lee, T.J., Kang, M.: Low temperature synthesis of α-alumina from aluminum hydroxide hydrothermally synthesized using [Al(C2O4)x(OH)y] complexes. Chem. Eng. J. **230**, 351–360 (2013). https://doi.org/10.1016/j.cej.2013.06.099
38. Ghogia, A.C., Machado, B.F., Cayez, S., Nzihou, A., Serp, P., Soulantica, K., Pham Minh, D.: Beyond confinement effects in Fischer-Tropsch Co/CNT catalysts. J. Catal. **397**, 156–171 (2021). https://doi.org/10.1016/j.jcat.2021.03.027
39. Yang, L.: CO2 conversion via reverse water-gas shift using multicomponent catalysts - University of Surrey (2021). https://openresearch.surrey.ac.uk/esploro/outputs/doctoral/99590523802346
40. Puig-Gamero, M., Pio, D.T., Tarelho, L.A.C., Sánchez, P., Sanchez-Silva, L.: Simulation of biomass gasification in bubbling fluidized bed reactor using aspen plus®. Energy. Conv. Manag. **235**, 113981 (2021). https://doi.org/10.1016/j.enconman.2021.113981
41. Kosky, P., Balmer, R., Keat, W., Wise, G.: Chap. 14 - Mechanical Engineering. In: Kosky, P., Balmer, R., Keat, W., Wise, G. (eds.) Exploring engineering (Fifth Edition), pp. 317–340. Academic (2021)
42. Živković, L.A., Pohar, A., Likozar, B., Nikačević, N.M.: Kinetics and reactor modeling for CaO sorption-enhanced high-temperature water–gas shift (SE–WGS) reaction for hydrogen production. Appl. Energy. **178**, 844–855 (2016). https://doi.org/10.1016/j.apenergy.2016.06.071
43. Seo, Y.-S., Seo, D.-J., Seo, Y.-T., Yoon, W.-L.: Investigation of the characteristics of a compact steam reformer integrated with a water-gas shift reactor. J. Power Sources. **161**, 1208–1216 (2006). https://doi.org/10.1016/j.jpowsour.2006.05.039
44. Elsaddik, M.: Hydrogen-rich syngas from steam gasification of cellulose in a biorefinery approach (2022). https://www.theses.fr/2022EMAC0016
45. Solli, K.-A., Thapa, K., Moldestad, R.: B.M.E.: Screening of kinetic rate equations for gasification simulation models (2018)
46. Abdelouahed, L., Authier, O., Mauviel, G., Corriou, J.P., Verdier, G., Dufour, A.: Detailed modeling of biomass gasification in dual fluidized bed reactors under aspen plus. Energy Fuels. **26**, 3840–3855 (2012). https://doi.org/10.1021/ef300411k
47. LaMont, D.C., Thomson, W.J.: Dry reforming kinetics over a bulk molybdenum carbide catalyst. Chem. Eng. Sci. **60**, 3553–3559 (2005). https://doi.org/10.1016/j.ces.2005.01.021
48. Klose, J., Baerns, M.: Kinetics of the methanation of carbon monoxide on an alumina-supported nickel catalyst. J. Catal. **85**, 105–116 (1984). https://doi.org/10.1016/0021-9517(84)90114-3
49. Reddy, G.K., Boolchand, P., Smirniotis, P.G.: Unexpected behavior of copper in modified ferrites during high temperature WGS reaction—aspects of Fe3+ ↔ Fe2+Redox Chemistry from Mössbauer and XPS studies. J. Phys. Chem. C. **116**, 11019–11031 (2012). https://doi.org/10.1021/jp301090d
50. Reddy, G.K., Gunasekara, K., Boolchand, P., Smirniotis, P.G.: Cr- and Ce-Doped ferrite catalysts for the high temperature water−gas shift reaction: TPR and Mossbauer Spectroscopic Study. J. Phys. Chem. C. **115**, 920–930 (2011). https://doi.org/10.1021/jp102959p

51. Abd El-Moemen, A., Karpenko, A., Denkwitz, Y., Behm, R.J.: Activity, stability and deactivation behavior of Au/CeO2 catalysts in the water gas shift reaction at increased reaction temperature (300°C). J. Power Sources. **190**, 64–75 (2009). https://doi.org/10.1016/j.jpowsour.2008.07.084
52. Kim, C.H., Thompson, L.T.: Deactivation of Au/CeOx water gas shift catalysts. J. Catal. **230**, 66–74 (2005). https://doi.org/10.1016/j.jcat.2004.10.004
53. Baraj, E., Ciahotný, K., Hlinčík, T.: The water gas shift reaction: catalysts and reaction mechanism. Fuel. **288**, 119817 (2021). https://doi.org/10.1016/j.fuel.2020.119817
54. Djinović, P., Batista, J., Pintar, A.: WGS reaction over nanostructured CuO–CeO2 catalysts prepared by hard template method: characterization, activity and deactivation. Catal. Today. **147**, S191–S197 (2009). https://doi.org/10.1016/j.cattod.2009.07.009
55. Si, R., Raitano, J., Yi, N., Zhang, L., Chan, S.-W., Flytzani-Stephanopoulos, M.: Structure sensitivity of the low-temperature water-gas shift reaction on Cu–CeO2 catalysts. Catal. Today. **180**, 68–80 (2012). https://doi.org/10.1016/j.cattod.2011.09.008
56. Gokhale, A.A., Dumesic, J.A., Mavrikakis, M.: On the mechanism of low-temperature water gas shift reaction on copper. J. Am. Chem. Soc. **130**, 1402–1414 (2008). https://doi.org/10.1021/ja0768237
57. Burch, R.: Gold catalysts for pure hydrogen production in the water–gas shift reaction: activity, structure and reaction mechanism. Phys. Chem. Chem. Phys. **8**, 5483–5500 (2006). https://doi.org/10.1039/B607837K
58. Dou, X., Veksha, A., Chan, W.P., Oh, W.-D., Liang, Y.N., Teoh, F., Mohamed, D.K.B., Giannis, A., Lisak, G., Lim, T.-T.: Poisoning effects of H2S and HCl on the naphthalene steam reforming and water-gas shift activities of Ni and Fe catalysts. Fuel. **241**, 1008–1018 (2019). https://doi.org/10.1016/j.fuel.2018.12.119
59. Pati, R.K., Lee, I.C., Hou, S., Akhuemonkhan, O., Gaskell, K.J., Wang, Q., Frenkel, A.I., Chu, D., Salamanca-Riba, L.G., Ehrman, S.H.: Flame synthesis of Nanosized Cu−Ce−O, Ni−Ce−O, and Fe−Ce−O catalysts for the water-gas shift (WGS) reaction. ACS Appl. Mater. Interfaces. **1**, 2624–2635 (2009). https://doi.org/10.1021/am900533p
60. Namiki, T., Yamashita, S., Tominaga, H., Nagai, M.: Dissociation of CO and H2O during water–gas shift reaction on carburized Mo/Al2O3 catalyst. Appl. Catal. A. **398**, 155–160 (2011). https://doi.org/10.1016/j.apcata.2011.03.029
61. Kundakovic, L., Mullins, D.R., Overbury, S.H.: Adsorption and reaction of H2O and CO on oxidized and reduced Rh/CeOx(111) surfaces. Surf. Sci. **457**, 51–62 (2000). https://doi.org/10.1016/S0039-6028(00)00332-0
62. Dongil, A.B., Pastor-Pérez, L., Escalona, N., Sepúlveda-Escribano, A.: Carbon nanotube-supported Ni–CeO2 catalysts. Effect of the support on the catalytic performance in the low-temperature WGS reaction. Carbon. **101**, 296–304 (2016). https://doi.org/10.1016/j.carbon.2016.01.103
63. Tomczyk, A., Sokołowska, Z., Boguta, P.: Biochar physicochemical properties: pyrolysis temperature and feedstock kind effects. Rev. Environ. Sci. Biotechnol. **19**, 191–215 (2020). https://doi.org/10.1007/s11157-020-09523-3
64. Akhil, D., Lakshmi, D., Kartik, A., Vo, D.-V.N., Arun, J., Gopinath, K.P.: Production, characterization, activation and environmental applications of engineered biochar: a review. Environ. Chem. Lett. **19**, 2261–2297 (2021). https://doi.org/10.1007/s10311-020-01167-7
65. Béguerie, T., Weiss-Hortala, E., Nzihou, A.: Calcium as an innovative and effective catalyst for the synthesis of graphene-like materials from cellulose. Sci. Rep. **12**, 21492 (2022). https://doi.org/10.1038/s41598-022-25943-3
66. Ghogia, A.C., Romero Millán, L.M., White, C.E., Nzihou, A.: Synthesis and growth of Green Graphene from Biochar revealed by magnetic properties of Iron Catalyst. ChemSusChem. **16**, e202201864 (2023). https://doi.org/10.1002/cssc.202201864
67. Rodriguez, J.A., Senanayake, S.D., Stacchiola, D., Liu, P., Hrbek, J.: The activation of gold and the water–gas shift reaction: insights from studies with model catalysts. Acc. Chem. Res. **47**, 773–782 (2014). https://doi.org/10.1021/ar400182c
68. Babatabar, M.A., Saidi, M.: Hydrogen production via integrated configuration of steam gasification process of biomass and water-gas shift reaction: process simulation and optimization. Int. J. Energy Res. **45**, 19378–19394 (2021). https://doi.org/10.1002/er.7087
69. Iriarte-Velasco, U., Sierra, I., Gutiérrez-Ortiz, M.A., Ayastuy, J.L.: Bioapatite derived from animal bones as support for environmentally concerned catalysts: WGS with suppressed methanation activity. J. Environ. Chem. Eng. **11**, 110677 (2023). https://doi.org/10.1016/j.jece.2023.110677
70. Liu, P., Rodriguez, J.A.: Water-gas-shift reaction on metal nanoparticles and surfaces. J. Chem. Phys. **126**, 164705 (2007). https://doi.org/10.1063/1.2722747
71. Shrestha, P., Chun, D.D., Kang, K., Simson, A.E., Klinghoffer, N.B.: Role of metals in biochar production and utilization in catalytic applications: a review. Waste Biomass Valor. **13**, 797–822 (2022). https://doi.org/10.1007/s12649-021-01519-6
72. Živković, L.A., Pohar, A., Likozar, B., Nikačević, N.M.: Reactor conceptual design by optimization for hydrogen production through intensified sorption- and membrane-enhanced water-gas shift reaction. Chem. Eng. Sci. **211**, 115174 (2020). https://doi.org/10.1016/j.ces.2019.115174
73. Arzamendi, G., Diéguez, P.M., Montes, M., Odriozola, J.A., Sousa-Aguiar, E.F., Gandía, L.M.: Methane steam reforming in a microchannel reactor for GTL intensification: a computational fluid dynamics simulation study. Chem. Eng. J. **154**, 168–173 (2009). https://doi.org/10.1016/j.cej.2009.01.035
74. Sheu, W.-J., Chu, C.-S., Chen, Y.-C.: The operation types and operation window for high-purity hydrogen production for the sorption enhanced steam methane reforming in a fixed-bed reactor. Int. J. Hydrog. Energy. **47**, 37192–37203 (2022). https://doi.org/10.1016/j.ijhydene.2021.11.112
75. Abbas, S.Z., Dupont, V., Mahmud, T.: Kinetics study and modelling of steam methane reforming process over a NiO/Al2O3 catalyst in an adiabatic packed bed reactor. Int. J. Hydrog. Energy. **42**, 2889–2903 (2017). https://doi.org/10.1016/j.ijhydene.2016.11.093
76. Chen, Y., Zhang, X., Chen, W., Yang, H., Chen, H.: The structure evolution of biochar from biomass pyrolysis and its correlation with gas pollutant adsorption performance. Bioresour. Technol. **246**, 101–109 (2017). https://doi.org/10.1016/j.biortech.2017.08.138